

# Anomalies in the electronic stopping of slow antiprotons in LiF

Guerda Massillon-JL,<sup>1</sup> Alfredo A. Correa,<sup>2</sup> Xavier Andrade,<sup>2</sup> and Emilio Artacho<sup>3,4,5</sup>

<sup>1</sup>*Instituto de Física, Universidad Nacional Autónoma de México, 04510 Mexico City, Mexico*

<sup>2</sup>*Quantum Simulations Group, Lawrence Livermore National Laboratory, Livermore, California 94550, USA*

<sup>3</sup>*CIC Nanogune and DIPC, Tolosa Hiribidea 76, 20018 San Sebastian, Spain*

<sup>4</sup>*Ikerbasque, Basque Foundation for Science, 48011 Bilbao, Spain*

<sup>5</sup>*Theory of Condensed Matter, Cavendish Laboratory, University of Cambridge, J. J. Thomson Ave, Cambridge CB3 0HE, United Kingdom*

(Dated: January 27, 2025)

We present first-principles theoretical calculations for the electronic stopping power (SP) of both protons and anti-protons in LiF. Our results show the presence of the Barkas effect: a higher stopping for positively charged particles than their negatively charged antiparticles. In contrast, a previous study has predicted an anti-Barkas effect (higher stopping for negative charges) at low velocity [Qi, Bruneval and Maliyov, *Phys. Rev. Lett.* **128**, 043401 (2022)]. We explain this discrepancy by showing that this anti-Barkas effect appears for highly symmetric trajectories and disappears when considering trajectories that better reproduce the experimental setup. Our low-velocity results show that the SP of both protons and anti-proton vanish for velocities under 0.1 a.u. .

Since the discovery of its thermoluminescent properties at the beginning of the 1950s [1], lithium fluoride (LiF), in addition to being a prototypical large band-gap insulator, it has been considered a crystal both of fundamental interest to understand the interaction of ionizing radiation with matter and of practical relevance as a dosimeter measuring absorbed dose in medical, space and occupational personal dosimetry and in environmental monitoring [2]. Studying the interaction of charged particles, like electrons, protons, and heavier ions, with matter is important in many areas of science and technology, including radiotherapy and nuclear and space activities.

Electronic stopping power (SP) is a quantity that defines the capability of a material to cause a charged particle to lose kinetic energy through electronic processes. SP is measured in energy per unit length traveled into matter. Several historic approximations, such as Fermi-Teller [3] for low-velocities, Bethe [4] at large velocities and linear response coincide in predicting a SP proportional to the square of the projectile charge ( $Z^2$ ). Under these analytic descriptions, the SP for a particle and its oppositely charged antiparticle should be the same. Nevertheless, Barkas and co-workers reported that for a similar initial velocity, the range of negative pions was longer than that of positive pions [5, 6]. Such results suggested that the stopping power for the positive projectile is larger than that for the negative counterpart [5]: the so-called ‘‘Barkas effect’’. They attributed this effect to the asymmetric polarization of the target electrons with respect to attraction and repulsion. The SP for protons and antiprotons in Si has been measured in the velocity range between 4.64 a.u. and 11 a.u. finding a contribution of order  $Z^3$  to the stopping power and the antiproton stopping power smaller than the proton by 19% at low-velocities and 3% at high-velocities, which confirmed the Barkas effect in solids [7].

Several experimental studies about SP of protons ( $H^+$ )

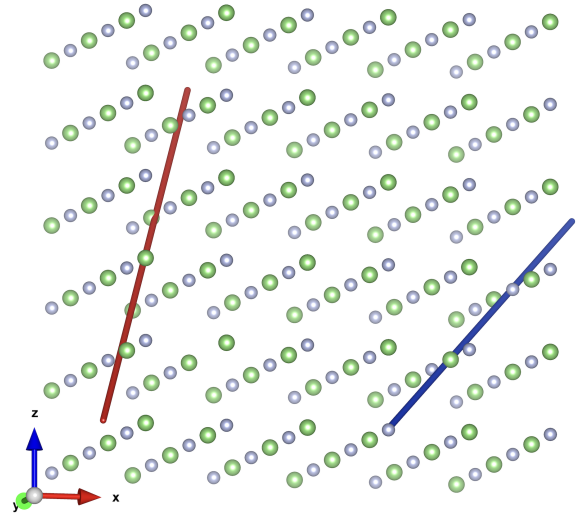


FIG. 1. LiF supercell of 216 atoms with two projectile trajectories, in a random incommensurate direction (red), and in a  $\langle 111 \rangle$  channeling (blue), for a small impact parameter  $p = 0.225\text{\AA}$ . The small impact parameter produces frequent repeating close approaches to host atoms. (The trajectories are 3-dimensional.) The gray and green balls represent F and Li, respectively.

in LiF have been reported [8–11], but to the best of our knowledge, only one for antiprotons ( $H^-$ ) by Møller et al. [9]. They experimentally investigated the SP for protons and antiprotons in LiF at velocities down to 0.3 a.u. and 0.4 a.u., respectively [9]. They reported differences in the SP for protons and antiprotons of around 50%-60%. They also concluded that the SP for the antiproton is almost linear with the velocity [9]. Measurements of the SP of low-velocity protons ( $v < 0.5$  a.u.) in LiF indicated that the SP vanishes below a certain velocity threshold of approximately 0.1 a.u [10, 11]. Theoretical studies based on real-time time-dependent density func-

tional theory (rt-TDDFT) simulations have confirmed these results [12–14]. From theory, a strict threshold is not expected but rather a smooth but strongly depressed SP at low velocities [15, 16] based on conservation arguments [17]. However, for low-velocity antiprotons where only rt-TDDFT simulated data exist, the results are still controversial. For antiprotons moving in  $\langle 100 \rangle$  channeling trajectories, a similar velocity threshold and the Barkas effect have been obtained from rt-TDDFT simulations using atomic orbitals [12]. In contrast, results from rt-TDDFT using Gaussian basis sets with the proton moving along a  $\langle 111 \rangle$  channeling trajectory suggested a negative Barkas effect (SP for antiprotons greater than that for protons) at velocities below 0.25 a.u. and, remarkably, no velocity threshold for antiprotons [14].

This letter presents SP results for protons and antiprotons in LiF via rt-TDDFT simulations within a pseudopotential plane-wave framework. Good agreement with available experimental data is obtained for both protons and antiprotons. A similar threshold effect is observed for both, with no trace of the reported anti-Barkas effect in the low-velocity limit, in apparent contradiction with the Gaussian basis simulation results.

Simulations via rt-TDDFT were performed through the open-source code Qball [18, 19] which is based on the plane-wave approach. In that code, the temporal evolution of the system’s total energy caused by the dynamic of the charged particles is described by the time-dependent Kohn-Sham equations. Optimized norm-conserving Vanderbilt (ONCV) pseudopotentials [20] were used to describe the interaction between valence electrons and core ions (Li and F ions with 3 and 7 valence electrons, respectively). For the proton, a local Coulomb pseudopotential for hydrogen was used, with the equivalent repulsive pseudopotential for the antiproton. The Perdew-Burke-Ernzerhof (PBE) functional [21] was used for the exchange-correlation (XC) functional. It is well known that PBE underestimates the band gap, which could affect proportionally the predicted velocity threshold. However, as we will show in this letter, it does not do it noticeably, since what we obtain is similar to experiments on the scale we are studying. The electronic wave function evolved through the enforced time reversal symmetry propagator [22]. The plane-wave basis set was the one corresponding to a 50 Hartree energy cutoff.

A time step,  $\Delta t = 1$  attosecond was used for velocities  $< 0.5$  a.u. and for greater velocities, a constant displacement of  $\Delta x = 0.005$  Å was set in each integration step ( $\Delta t = \Delta x/v$ ). Both projectiles were moved in a direction incommensurate with the crystalline lattice [23] at constant velocity through a  $3 \times 3 \times 3$  supercell of a pristine LiF containing 216 atoms (Fig.1 1). The geometry of the pristine supercell was previously optimized at the hybrid PBE0 level rendering a lattice constant of 4.028 Å [24]. For the calculation of electronic stopping power, the host atoms were frozen during the simulation,

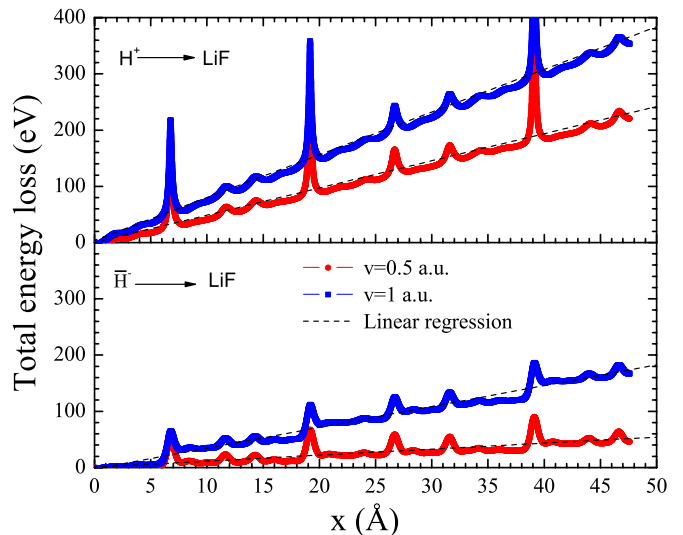


FIG. 2. Electronic total energy gain (projectile’s kinetic energy loss) versus projectile displacement  $x$  along an incommensurate trajectory, for proton/antiproton (upper/lower panel), and for  $v = 0.5$  a.u./1.0 a.u. (red/blue color).

thereby avoiding nuclear stopping effects by construction. The SP  $S_e = dE/dx$  in this work was obtained as the slope from a linear regression of the total electronic energy versus the projectile displacement  $x$  (see Fig. 2). Among different trajectory sampling techniques discussed in the literature for SP averaging [23, 25–27] the incommensurate-trajectory method has been shown to be the simplest and satisfactorily accurate. Atomic units are used for  $v$  and eV/Å for  $S_e$  as customary in this field (1 Hartree/Bohr = 51.422 eV/Å).

Figure 3 displays our rt-TDDFT results of the SP for protons and antiprotons in LiF as a function of the projectile velocity. Note that no negative Barkas effect is observed in the SP for antiprotons, as the antiproton stopping is consistently lower than proton stopping. Compared with the experiments [9–11], we find good agreement with the simulation for the proton where a velocity threshold of  $v \sim 0.1$  a.u. is also obtained. Relative to the SRIM [28, 29] and PSTAR [30, 31] data, the maximum SP obtained in the simulation is smaller by about 2 eV/Å. This discrepancy is due to the  $1s$  electrons of F being frozen into its pseudopotential [25, 32]. Concerning the antiproton, note a slight difference (or shift) with the experiment which is relatively more pronounced at lower velocities. This discrepancy can presumably be associated with the uncertainties in the thickness of the foils used in the experiment [9], which could result in a systematic error.

Furthermore, similarly to the protons, a velocity threshold, where the SP vanishes, exists for the antiprotons. For the antiprotons, a velocity threshold at around  $v = 0.2$  a.u. is obtained. Such a result contrasts with the hypothesis that the velocity threshold where the SP

vanishes for the antiprotons should be smaller than for protons [33].

To understand the negative Barkas effect reported by Qi et al. [14], we performed simulations for antiprotons moving at several constant velocities along the  $\langle 111 \rangle$  direction in channeling trajectories with a low impact parameter  $p = 0.225 \text{ \AA}$  relative to the fluorine or lithium sites. This result is shown in Fig. 3 and, interestingly, the negative Barkas effect is observed in the velocity range studied and a local maximum at velocity below  $v = 0.3 \text{ a.u.}$ , as also reported by Qi et al. for the smallest impact parameter  $p = 0.225 \text{ \AA}$  (see inset of Fig. 2 from Ref. [14]).

According to the Fermi-Teller theory regarding capture of mesons [3], the presence of a low negative charge moving within one lattice parameter from an atom in an insulator can generate a gap state, which has been confirmed by calculations of Solleder et al. who showed a localised state in the LiF gap caused by the repulsive potential of the antiproton [33]. They did not find an in-gap state for the proton. Based on the Fermi-Teller approach, at low velocity, there would exist a critical distance (Fermi-Teller radius,  $r_{\text{FT}} = 0.639/Za_B$ ) where the antiproton will be captured by the fluorine, provoking a resonance that locally enhances the energy loss by the antiproton [3]. This extra energy loss may explain the anti-Barkas effect observed on the SP calculated in channeling trajectories reported by Qi et al. [14] at low velocity and low impact parameter. An oscillatory gap state characteristic of an antiproton traveling at repeated close approaches would lower the effective large gap of LiF, which is otherwise responsible for the threshold behavior. Since this state sits at the Fermi level, it would be able to carry electrons from the valence to the conduction band in analogy to the effect termed ‘electron elevator’ reported in Ref. [34] and more generally modeled in Ref. [35], providing a mechanism for sub-threshold behavior observed for the channeling trajectories assumed by Qi et al.

To model the subthreshold structure for low-impact parameters and at low velocity ( $v < 0.2 \text{ a.u.}$ ), we use the theory developed by Horsfield et al. [35], which was initially designed to capture the effect of a gap level formed by a slow projectile on the electronic stopping in insulators. The mentioned gap level in LiF observed for the antiproton (and not the proton) [33] makes the Horsfield model suitable to model the antiproton electronic SP. This perturbative model establishes that a general gap level (carried by the slow projectile) generates an additive stopping  $S_d$  on top of the normal interband (valence-conduction) stopping power.  $S_d$  is a function of (i) the energy distance  $|\bar{\epsilon}_d|$  below/above the unoccupied/occupied band with a electronic density of states  $\mathcal{D}$ , (ii) the amplitude of this oscillation  $\eta$ , and (iii) the

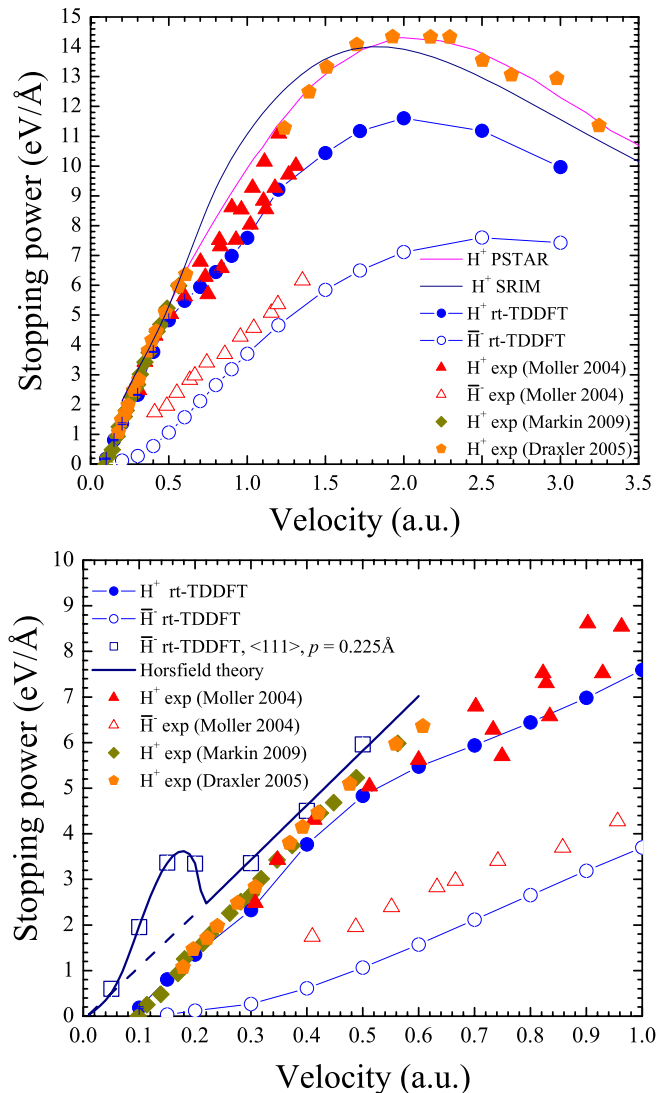


FIG. 3. Electronic stopping power for protons (filled symbols) and antiprotons (open symbols) travelling through LiF versus projectile velocity. Upper panel: Results obtained via rt-TDDFT simulations are compared with reported experimental results and data from SRIM and PSTAR. Lower panel: Simulation results for low-velocity proton and antiproton averaged trajectories are compared with a  $\langle 111 \rangle$  channelling trajectory for antiprotons with an impact parameter (closest approach to fluorine atom) of  $p = 0.225 \text{ \AA}$ . The dark blue continuous line shows the Horsfield model, with contributions from the  $S_d$  formula in the text, which generates the shoulder at around 1.5 a.u., plus from an adjusted linear contribution from interband stopping (dashed extrapolated line).

passing frequency  $\omega$ .

$$S_d \propto \sum_{\ell} \ell |I_{\ell}(\eta/\hbar\omega)|^2 \mathcal{D}(\bar{\epsilon}_d + \ell\hbar\omega), \quad (1)$$

where  $I_{\ell}(x) = \frac{1}{2\pi} \int_0^{\pi} \frac{\sin(\ell u + x \sin u)}{\ell + x \cos u} \sin u \, du$  which we denominate the Horsfield function. Note that  $\omega$ , inverse of a passing time, is proportional to the velocity  $\omega = 2\pi v/\lambda$ .

A single (conduction) parabolic band of width  $\omega$  is assumed,  $\mathcal{D}(\varepsilon) \propto \sqrt{\varepsilon}$  with a soft energy cutoff (band width)  $\Omega$ . We fix  $\eta$  and  $\bar{\varepsilon}_d$  at 12 eV and  $-6$  eV, which respectively correspond to the amplitude and average relative to the bottom of the conduction band, based on Fig. 3a of Ref. [33] for the antiproton gap level. A non-linear least-square fitting results in  $\lambda = 0.15 \text{ \AA}$ ,  $\Omega = 3.84 \text{ eV}$ . (For these parameters,  $\ell \geq 2$  contributions are vanishingly small.) The total electronic stopping power from this simple model ( $S_d$  plus an adjusted linear interband stopping) is depicted in Fig. 3b.

Subthreshold behavior for the antiproton is only observed for these unique trajectories (channeling and small impact parameter), and our results for the average stopping power do not reveal subthreshold features. In this regard, we attribute the discrepancy with Ref. [14] to a different way of sampling trajectories. (The plane wave methods are more amenable to simulations at random directions thanks to periodic boundary conditions.) This illustrates that the random direction (or incommensurate) averaging method is not necessarily equivalent to sampling impact parameters for strict channeling trajectories over a crossing plane. We interpreted that such theoretically described subthreshold behavior would not be directly observed in simple experiments since projectile trajectories with small impact parameters (in a channel) would be disfavored by nuclei scattering.

In conclusion, by comparing systematic simulations of the electronic stopping power of protons and antiprotons, we find a positive Barkas effect; that is, the positively charged projectile has larger electronic stopping power than the negatively charged counterpart across the investigated velocity range. Both projectiles have a similar threshold velocity within the simulation's resolution (at  $v = 0.1 \text{ a.u.}$ ). The proton stopping is five or more times larger than the antiproton stopping at low velocity. The relative difference reduces to less than half near the maxima (at  $v = 2.0 \text{ a.u.}$  and  $2.5 \text{ a.u.}$ , respectively). At higher velocities ( $>3.5 \text{ a.u.}$ ), we expect the stopping values of protons and antiprotons to eventually converge when linear theory and the Bethe limit become more exact. Accurate reporting at such high velocities would require simulations with more explicit valence electrons within the pseudopotential method. The antiproton results are systematically lower than Møller's experiment by  $\sim 1 \text{ eV/\AA}$ . We explain the apparent discrepancy between the theoretical results of the previous first principles by combining arguments regarding the trajectory sampling method and a physical effect characteristic of small impact parameter channeling trajectories.

*Acknowledgments.* The authors thank Irving Carlos Álvarez Castillo from DGTIC-UNAM for technical support. We acknowledge computational support from Atlas and Hyperion DIPC, Spain and Mitzli UNAM Mexico through grant ref. LANCAD-UNAM-DGTIC-334. This project is partially supported by the European Commis-

sion Horizon MSCA-SE Project MAMBA (Grant No. 101131245). GMJL's sabbatical leave at CIC-Nanogune in Spain was funded by DGAPA UNAM. AAC and XA work was supported by the Center for Non-Perturbative Studies of Functional Materials Under Non-Equilibrium Conditions (NPNEQ) funded by the Computational Materials Sciences Program of the US Department of Energy, Office of Science, Basic Energy Sciences, Materials Sciences and Engineering Division and performed under the auspices of the US Department of Energy by Lawrence Livermore National Laboratory under contract DE-AC52-07NA27344. EA acknowledges funding from the Spanish MCIN/AEI/10.13039/501100011033 through grants PID2019-107338RB-C61 and PID2022-139776NB-C65, as well as a María de Maeztu award to Nanogune, Grant CEX2020-001038-M.

- 
- [1] S. Daniels, C. Boyd, and D. Saunders, *Science* **117**, 343 (1953).
  - [2] G. Massillon-JL, I. Gamboa-deBuen, and M. Brandan, *J. Phys. D: Appl. Phys.* **40**, 2584 (2007).
  - [3] E. Fermi and E. Teller, *Phys. Rev.* **72**, 399 (1947).
  - [4] U. Fano, *Ann. Rev. Nucl. Sci.* **13**, 1 (1963).
  - [5] F. Smith, W. Birnbaum, and W. H. Barkas, *Phys. Rev.* **91**, 765 (1953).
  - [6] W. H. Barkas, W. Birnbaum, and F. M. Smith, *Phys. Rev.* **101**, 778 (1956).
  - [7] L. Andersen, P. Hvelplund, H. Knudsen, S. Møller, J. Pedersen, E. Uggerhøj, K. Elsener, and E. Morenzoni, *Phys. Rev. Lett.* **62**, 1731 (1989).
  - [8] M. Bader, R. Pixley, F. Mozer, and W. Whaling, *Phys. Rev.* **103**, 32 (1956).
  - [9] S. P. Møller, A. Csete, T. Ichioka, H. Knudsen, U. I. Uggerhøj, and H. Andersen, *Phys. Rev. Lett.* **93**, 042502 (2004).
  - [10] M. Draxler, S. Chenakin, S. Markin, and P. Bauer, *Phys. Rev. Lett.* **95**, 113201 (2005).
  - [11] S. Markin, D. Primetzhofer, and P. Bauer, *Phys. Rev. Lett.* **103**, 113201 (2009).
  - [12] J. M. Pruneda, D. Sánchez-Portal, A. Arnau, J. I. Juaristi, and E. Artacho, *Phys. Rev. Lett.* **99**, 235501 (2007).
  - [13] M. A. Zeb, J. Kohanoff, D. Sánchez-Portal, and E. Artacho, *Nucl. Instrum. Meth. B* **303**, 59 (2013).
  - [14] X. Qi, F. Bruneval, and I. Maliyov, *Phys. Rev. Lett.* **128**, 043401 (2022).
  - [15] E. Artacho, *J. Phys. Condens. Matter* **19**, 275211 (2007).
  - [16] N. Forcellini and E. Artacho, *Phys. Rev. Research* **2**, 033151 (2020).
  - [17] R. Ullah, F. Corsetti, D. Sánchez-Portal, and E. Artacho, *Phys. Rev. B* **91**, 125203 (2015).
  - [18] "Qball Software," <https://github.com/LLNL/qball>, accessed: 2024-07-05.
  - [19] E. W. Draeger, X. Andrade, J. A. Gunnels, A. Bhatele, A. Schleife, and A. A. Correa, *J. Parallel Distr. Comp.* **106**, 205 (2017).
  - [20] D. Hamann, *Phys. Rev. B* **88**, 085117 (2013).
  - [21] J. P. Perdew, K. Burke, and M. Ernzerhof, *Phys. Rev. Lett.* **77**, 3865 (1996).

- [22] A. Castro, M. A. Marques, and A. Rubio, *J. Chem. Phys.* **121**, 3425 (2004).
- [23] A. A. Correa, *Comp. Mater. Sci.* **150**, 291 (2018).
- [24] G. Massillon-Jl, C. S. Johnston, and J. Kohanoff, *J. Phys. Condens. Matter* **31**, 025502 (2018).
- [25] R. Ullah, E. Artacho, and A. A. Correa, *Phys. Rev. Lett.* **121**, 116401 (2018).
- [26] B. Gu, B. Cunningham, D. Muñoz-Santiburcio, F. Da Pieve, E. Artacho, and J. Kohanoff, *J. Chem. Phys.* **153**, 034113 (2020).
- [27] L. Ward, B. Blaiszik, C.-W. Lee, T. Martin, I. Foster, and A. Schleife, *npj Computational Materials* **10** (2024), 10.1038/s41524-024-01374-8.
- [28] <http://srim.org>, accessed: 2024-07-05.
- [29] J. F. Ziegler, M. D. Ziegler, and J. P. Biersack, *Nucl. Instrum. Methods Phys. Res. B* **268**, 1818 (2010).
- [30] <https://physics.nist.gov/PhysRefData/Star/Text/PSTAR.html>, accessed: 2024-07-05.
- [31] M. Berger, J. Coursey, and M. Zucker, “ESTAR, PSTAR, and ASTAR: Computer Programs for Calculating Stopping-Power and Range Tables for Electrons, Protons, and Helium Ions (version 1.21),” (1999).
- [32] A. A. Shukri, F. Bruneval, and L. Reining, *Phys. Rev. B* **93**, 035128 (2016).
- [33] B. Solleder, L. Wirtz, and J. Burgdörfer, *Phys. Rev. B* **79**, 125107 (2009).
- [34] A. Lim, W. Foulkes, A. Horsfield, D. Mason, A. Schleife, E. Draeger, and A. Correa, *Phys. Rev. Lett.* **116**, 043201 (2016).
- [35] A. P. Horsfield, A. Lim, W. Foulkes, and A. A. Correa, *Phys. Rev. B* **93**, 245106 (2016).